CONFERENCE PRE-PRINT

MATERIAL SELECTION FOR MIRROR SUBSTRATES EXPOSED TO HIGH-POWER LASER BEAMS IN THE ITER TRITIUM-MONITOR DIAGNOSTIC

A. Huber[1], G. Sergienko[1], I. Ivashov[1], Ph. Andrew[2], J. Assmann[1], D. Castano-Bardawil[3], A. De Schepper[1], S. Friese[1], R. Greven[4], D. Kampf[5], Y. Krasikov[1], Ph. Mertens[6], K. Mlynczak[1], G. Offermanns[4], M. Schrader[1], D. Van Staden[5], A. Terra[1], Xi Jiang[2], M. Zlobinski[1], V. Huber[7], A. Reutlinger[5], S. Brezinsek[1], Ch. Linsmeier[1]

[1]Forschungszentrum Jülich GmbH, Institute of Fusion Energy and Nuclear Waste Management–Plasma Physics, Germany
[2]ITER Organization, Route de Vinon, CS 90 046, 13067 Saint-Paul-lez-Durance, France
[3]Laboratory for Plasma Physics, Royal Military Academy Brussels, (LPP-ERM/KMS), TEC Partner, Belgium
[4]Forschungszentrum Jülich GmbH, Institute of Technology and Engineering, 52425 Jülich, Germany
[5]KTO Kampf Telescope Optics GmbH
[6]FUSE-L Fusion Specific Expertise-Liege, Route du Condroz 111B, B-4031 Liège, Belgium
[7]Forschungszentrum Jülich GmbH, Supercomputing Centre, 52425 Jülich, Germany

Abstract

The ITER T-monitor diagnostic employs high-power laser pulses and metallic mirrors for in-situ measurements of tritium retention on plasma-facing components. The optical system must operate under extreme conditions, including high localized power densities, elevated background temperatures, nuclear radiation, and strong magnetic fields, while maintaining optical quality. This study evaluates candidate mirror substrate materials using a simplified thermoelastic–thermoplastic model and finite-element simulations. Critical heat-flux factors were derived for three operational limits: (i) the onset of permanent damage, defined as plastic deformation when laser-induced stresses reach the material yield strength, (ii) a maximum allowable gold-coating temperature of 520 °C, and (iii) optical surface deformation limited to $\lambda/8$ at $\lambda = 1.07$ µm. Both uniform and Gaussian laser profiles were considered. For the most demanding operational scenarios, simulations confirmed that temperature rises remain below the plastic deformation threshold and surface deformations have negligible impact on optical performance. The results provide material selection guidelines and demonstrate that the proposed optical design ensures reliable T-monitor operation under ITER's nuclear environment.

1. Introduction

The ITER (International Thermonuclear Experimental Reactor) project [1] represents a major step toward fusion energy, requiring advanced diagnostics to ensure safe, efficient, and sustained operation. Among these, the T-monitor diagnostic plays a critical role by providing in-situ measurements of tritium retention on plasma-facing components inside the vacuum vessel. Accurate monitoring of tritium is essential because ITER is a licensed nuclear facility with a strict retention limit of 1 kg, of which only 700 g is allowed inside vessel components after accounting for cryopump inventory and measurement uncertainty [2].

To meet these requirements, the T-monitor uses laser-induced desorption (LID) combined with residual gas analysis (RGA) [3] to determine the local tritium content with high spatial resolution without removing components from the vessel. A key element of this system is the coaxial optical delivery and observation path, which must reliably transport high-power laser pulses to the divertor target and enable coaxial VIS/NIR imaging of the laser-heated surface.

The in- and ex-vessel optical system consists of a series of metallic mirrors (M1–M29) that guide the laser beam through extreme conditions, including elevated temperatures, neutron and gamma radiation, strong magnetic fields, and high laser power densities. Transient thermal stresses from laser exposure can cause surface roughening, plastic yielding, coating delamination, or deformation, potentially degrading the optical performance and limiting the diagnostic reliability.

In its most demanding operational mode, the T-monitor laser delivers millisecond pulses at up to 60 Hz, generating a localized heating of the mirrors. Certain mirrors, such as M4 and M5 (see §2.1 below), experience the highest power densities (≈7.85 kW/cm²) which coincide with the smallest laser spot size, making them particularly sensitive to thermomechanical effects.

This paper evaluates mirror substrate materials for the ITER T-monitor system. A simplified thermoelastic–thermoplastic model using the infinite half-space approximation estimates critical heat flux based on damage limits due plastic deformation, $\lambda/8$ optical deformation, and gold coating temperature constrains. These results are compared with transient thermal and deformation simulations, including multi-pulse loading. The study identifies suitable materials, assesses safety margins, and informs the optical design to ensure reliable tritium diagnostics in ITER's nuclear environment. The paper is structured as follows: Section 2 describes the optical design and mechanical layout. Section 3 presents the thermal stress and deformation model. Section 4 applies the model to Gaussian laser loading. Section 5 analyses multi-pulse operation. Section 6 summarizes key results and mirror performance. Section 7 outlines material selection, including baseline and backup options.

2.0 Optical Design and Mechanical Layout

The ITER T-monitor diagnostic system (55.GC) is installed in Equatorial Port 17, with optical components distributed both in-vessel (inside the Diagnostic Shielding Module, DSM#2) and in ex-vessel regions (Interspace Support Structure (ISS) area), bioshield, Port Cell Support Structure (PCSS), and Tritium Building). Figure 1 provides an overview of the T-monitor optical system, including the in-vessel mirror arrangement, the mechanical layout of the mirror boxes, and the

protective shutter system. The figure illustrates the optical path for high-power laser delivery and coaxial VIS/NIR observation of the divertor target, highlighting the relative positions and orientations of the mirrors within the vacuum vessel as well as in the ex-vessel region.
The optical path must maintain precise alignment despite differential thermal expansion across these areas. Alignment is ensured by the Fast Scanning Mirror Unit (FSMU) in the ISS and an optical dog-leg arrangement. The same coaxial path is used for both laser injection and light collection by a VIS camera, an NIR camera, and a three-channel pyrometer. The entrance pupil is defined at the ISS tip/tilt mirror (M7, 56 mm aperture), and the optics are designed to achieve a diffraction-limited spot radius of 120 µm at the divertor target.

2.1 In-Vessel Optics

The in-vessel optical system comprises six mirrors (M1–M6) arranged in front and rear mirror boxes and a vacuum window (see Fig.1a). The mirror M3 has a toroidal shape; the others are flat. Dust and contamination are mitigated via closed ducts and a protective shutter. Temperature monitoring is provided by Type N thermocouples with mineral-insulated cables. Thermal and optical performance were verified using ANSYS– Zemax OpticStudio simulations. A pneumatic, water-cooled shutter protects M1 and the back of the shutter blade can be heated to 1200°C for calibration [4].

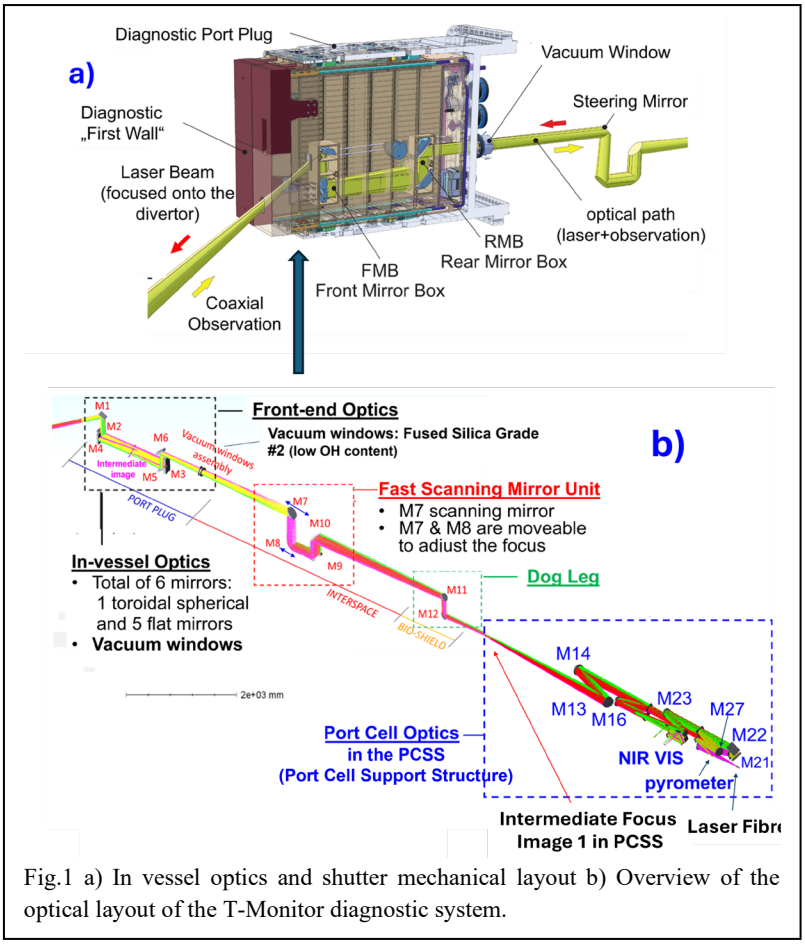

Fig.1 a) In vessel optics and shutter mechanical layout b) Overview of the optical layout of the T-Monitor diagnostic system.

2.2 Ex-Vessel Optics

The ex-vessel optical system provides beam transport, alignment, and diagnostic functions outside the vacuum vessel, ensuring reliable laser delivery and signal collection under ITER's operational conditions. It connects the in-vessel mirrors to external components, while maintaining beam quality and enabling precise measurements through a combination of scanning units, alignment optics, and diagnostic instruments.

- **FSMU in ISS:** Four mirrors (M7–M10) provide fast scanning (up to 60 Hz) and fine alignment. The parabolic mirrors M8 and M10 (f = 4441 mm) focus the beam.
- **Bioshield:** A two-mirror cold dog-leg (M11, M12 on hexapod mounts) ensures a precise beam alignment.
- **PCSS:** Combines VIS (600–900 nm, 0.1 mm resolution) and NIR (2.1–2.3 µm, high-speed thermal imaging) cameras, with calibration at the Intermediate Focus Image 1.
- **Tritium Building:** Houses a 60 kW, 1070 nm Ytterbium fiber laser and a three-channel pyrometer (1.4–2.0 µm) using fiber-coupled optics for multi-wavelength temperature measurement of the divertor hotspot.

More details about the T-monitor diagnostic can be found in [5,6].

3.0 Simplified Thermal Stress and Deformation Model for Laser-Irradiated Mirror Materials

High-power laser irradiation can cause transient surface heating, inducing significant stresses in the mirrors. These stresses may lead to surface roughening, yielding (plastic deformation when the stress exceeds the yield strength), or fracture. An accurate stress determination for specific materials and loads often requires a time-dependent 3D analysis. However, in many cases, a simplified one-dimensional model provides a good estimate of the peak stress.
The temperature rise after a laser pulse of duration τ depends on how deeply heat diffuses during the pulse. For short pulses, the thermal diffusion length is:

$$d = \sqrt{\alpha\tau} \qquad (1)$$

where $\alpha = \frac{k}{\rho C_p}$ is the thermal diffusivity of the material and τ_p is the laser pulse duration, determines the depth over which heat penetrates during the pulse. For CuCrZr metal with $\alpha \approx 0.9\times10^{-4}$ m²/s and pulse durations of of $\tau = 1\ ms$ and $3ms$, the thermal diffusion length is approximately 300 µm and 520 µm, respectively. The laser spot on the mirrors has a radius R that varies from 14 mm (for mirror M4) to 30 mm. Thus, the normalized diffusion length $x = \sqrt{at}/R$ is smaller than 0.037 for all mirrors at 3ms pulse duration.

At the same time, the thermal diffusion lengths for τ = *1 ms* and *3 ms* are much larger than the optical skin depth, which is on the order of *10–20 nm*, allowing a surface-heating approximation to be applied.
This paragraph introduces a simplified model that accounts for finite heat penetration depths based on the infinite half-space approximation to estimate the stress and deformation of different mirror material options. The transverse stresses in both orthogonal directions parallel to the mirror surface are expressed as [7,8]

$$\sigma_t = -\frac{E\alpha_L \Delta T}{1-\nu} \tag{2}$$

where E is the elastic modulus, α_L is the linear coefficient of thermal expansion, ΔT is the temperature difference at the surface from a stress-free reference temperature and ν is Poisson's ratio. The simplification used here involves imposing the boundary condition that the normal stress — the stress component acting perpendicular to a surface — at the free surface is zero. In the near-surface region of the metal, this normal stress is relieved in a short time compared to the time required for thermal diffusion to reduce the temperature. Using temperature equations given by Carslaw & Jaeger [11], the temperature increase ΔT at the end of the heating pulse can be defined as:

$$\Delta T = \frac{2}{\kappa}\sqrt{\frac{\alpha}{\pi}}\, q\sqrt{\tau} = \frac{2}{\kappa}\sqrt{\frac{\alpha}{\pi}}\, Q_f, \tag{3}$$

where $Q_f = q\sqrt{\tau}$ is the heat flux factor, q - heat flux on the surface and τ - heating pulse duration $\alpha = \frac{k}{C_p\,\rho}$ is the thermal diffusivity, κ is the thermal conductivity, C_p is specific heat capacity and ρ is the density of the material. The critical heat factor for mirrors can be calculated from Eqs. (1) and (2), assuming that σ_t has reached the critical value $[\sigma]$. It can be expressed as:

$$Q_{f,[\sigma]} = \frac{\kappa[\sigma]\,(1-\nu)}{2E\alpha_L}\sqrt{\pi/\alpha}\,, \tag{4}$$

where $[\sigma]$ is the allowable stress: yield stress for ductile materials and ultimate compressive stress for brittle materials. This value represents the threshold at which the mirror experiences permanent damage at the central point of the laser heated area. Note that, while $Q_{f,[\sigma]}$ is an exact upper bound for the peak stress for most mirror geometries made of ductile materials, it serves only as an indicative value for mirrors made of brittle materials due to the presence of tensile stresses at the border of the laser spot. On top of that, to prevent delamination of the Au layer from the substrate, which would lead to the failure of the reflective surface, the surface temperature of the gold coating must stay below 520°C (roughly the half of the melting temperature of gold is 1039 °C**)**. The critical heat flux factor for a temperature increase to ΔT_{max} =520°C is:

$$Q_{f,\Delta T=520°C} = \frac{\kappa}{2}\sqrt{\frac{\pi}{\alpha}}\,\Delta T_{max} = \frac{\sqrt{\pi\,\kappa\,c_p\,\rho}}{2}\,\Delta T_{max} \tag{5}$$

However, the optical quality may degrade before a permanent damage occurs. For the T-monitor mirrors to maintain an acceptable optical performance, the surface deformation must remain below λ/8 for laser operation at λ = 1.07 μm to avoid the optical distortion.
The surface deformation or axial displacement (displacement in the direction normal to the surface) of the mirror surface due to thermal expansion during the laser exposure is given by Eq. (A7)

$$v(\tau) = \frac{(1+\nu)}{(1-\nu)}\alpha_L \int_0^\infty \Delta T(z,\tau)dz = \frac{(1+\nu)}{(1-\nu)}\alpha_L \frac{\sqrt{\pi}}{2}\sqrt{\kappa\tau}\,\Delta T(0,\tau) = \frac{(1+\nu)}{(1-\nu)}\alpha_L \frac{\kappa}{K} q\tau = \frac{(1+\nu)}{(1-\nu)}\,\frac{\alpha_L}{c_p\rho}\,q\tau \tag{6}$$

This is an optimistic estimation for the displacement of the surface of an infinite half-space:

$$v(\tau) = \frac{1+\nu}{1-\nu}\frac{\alpha_L}{C_p\,\rho}q\tau \tag{7}$$

Assuming a surface displacement of $v(\tau)$=λ/8 in Eq. (7), one can derive the expression for the critical heat-flux factor. The critical heat-flux factor $q\sqrt{\tau}$ required to produce a deformation of λ/8 is then given by:

$$Q_{f,\lambda/8} = \frac{1-\nu}{1+\nu}\frac{C_p\,\rho\,\lambda}{8\,\alpha_L\sqrt{\tau}}.. \tag{8}$$

4.0 Critical Heat Flux and Surface Deformation of Mirrors under Gaussian Laser Irradiation

The stress distribution depends strongly on the laser's spatial profile. A Gaussian beam produces a peak temperature and stress at the center with smoothly decreasing radial gradients, whereas uniform heat exposure results in a nearly uniform temperature across the surface, leading to different stress patterns. Understanding these stress patterns is critical for estimating surface deformation and ensuring the optical performance of mirrors under high-power laser exposure.
This section introduces the temperature distribution produced by pulsed laser heating with a Gaussian heat-flux profile. For a Gaussian laser beam with an absorbed power flux density $q(r) = q_0 exp\,(-\frac{1}{2}\left(\frac{nr}{R}\right)^2)$, the temperature rise at the end of a pulse is given by Eq. (B8):

$$\Delta T_{Gauss}(r,z,\tau) = T(r,z,\tau) - T_0 = \frac{\bar{q}R^2}{4k}\sqrt{\frac{\alpha}{\pi}}\int_0^\tau \frac{dt\prime}{\sqrt{t'}\left(\frac{R^2}{2n^2}+\alpha t\prime\right)} exp\left[-\frac{z^2}{4\alpha t'} - \frac{r^2}{4\left(\frac{R^2}{2n^2}+\alpha t\prime\right)}\right] \tag{9}$$

where T_0 is the initial temperature, α is the thermal diffusivity, $\bar{q}$ is the power density averaged over the laser spot, $q_0 = \bar{q}\,n^2/2$ is the peak surface power flux (as shown in Eq. (B2)), R is the beam waist at $e^{-n^2/2}$ (for *n=2, 1/e²*) intensity, n is the Gaussian shape parameter and τ is the pulse duration. At the surface centre (*r=0, z=0*) the solution reduces to:

$$\Delta T_{Gauss}(0,0,\tau) = \frac{2}{\kappa}\sqrt{\frac{\alpha}{\pi}}\,\bar{q}\,\sqrt{\tau}\;F_{Gauss}(x,n) = \frac{2}{\kappa}\sqrt{\frac{\alpha}{\pi}}\,Q_f\;\;F_{Gauss}(x,n) \tag{10}$$

where $x = \sqrt{\alpha t}/R$ is the normalized diffusion length. The factor $F_{Gauss}(x,n)$ accounts for the difference between the central temperature for a Gaussian power distribution and that for a uniform heat-flux distribution (Eq. (3)), when both distributions have the same average power density.

In experiments, the maximum heat-flux factors are measured at the center of the laser spot rather than averaged over the entire spot. Therefore, the product $\bar{q}\sqrt{\tau}\;\cdot F_{Gauss}(x,n) = Q_f\;\cdot F_{Gauss}(x,n)$ represents the maximum heat-flux factor at the spot center. Under this definition, Eqs. (3) and (10) yield the same temperature increase and correspond to identical stress values. This confirms that our general equation (9) for the temperature increase is consistent and correctly reproduces the approximate solution in Eq. (3) under the same assumptions.

When the thermal diffusion length during the pulse, $d = \sqrt{\alpha\tau}$, is much smaller than the beam waist radius R, we have:

$$\lim_{x\to 0+} F_{Gauss}(x,n) \;= \frac{n^2}{2}. \tag{11}$$

For $n=2$, $q_0 = \bar{q}\,F_{Gauss}(x,2) \;= 2\;\cdot \bar{q}$ which corresponds to the power flux density

$$q(r) = q_0 exp\;\left(-2\left(\frac{r}{R}\right)^2\right), \tag{12}$$

Accordingly, the critical heat factor ($Q_f^{Gauss,peak} = Q_f \cdot F_{Gauss}(0,2)$) for mirrors at the spot centre can be expressed as:

$$Q_{f,[\sigma]}^{Gauss,peak} = \frac{\kappa[\sigma]\,(1-\nu)}{2E\alpha_L}\sqrt{\pi/\alpha}\,. \tag{13}$$

Analogous to paragraph 3, we calculate here the critical heat-flux factor for mirrors when transfer stresses σ_t reaches the yield strength [σ].

The axial displacement $v(r,0,\tau)$- $v(R,0,\tau)$ can be obtained from Eq. (A7) and the integration of the Eq. (9) over z and expressed as follows:

$$v(r,0,\tau) - v(R,0,\tau) \approx\; -\frac{(1+\nu)}{(1-\nu)}\alpha_L \int_0^\infty \Delta T(r,z,\tau)dz = F_{Gauss}(x,n)\frac{(1+\nu)}{(1-\nu)}\frac{\alpha_L}{C_p\rho}\bar{q}\tau\;\; e^{\frac{-nr^2}{2R^2}} \tag{14}$$

which has the maximum value at the center of the laser spot taking into account that $v(0,0,\tau) \gg v(R,0,\tau)$:

$$v_{max} = v(0,0,\tau) \approx\; -\frac{(1+\nu)}{(1-\nu)}\alpha_L \int_0^\infty \Delta T(r,z,\tau)dz \approx F_{Gauss}(x,n)\cdot\frac{(1+\nu)}{(1-\nu)}\;\frac{\alpha_L}{C_p\rho}\,\bar{q}\tau \tag{15}$$

From this, the critical heat flux factor, $F_{Gauss}(x,n)\cdot\bar{q}\sqrt{\tau} = q_0\sqrt{\tau}$, required to achieve a $\lambda/8$ deformation at the laser spot centre is given by

$$Q_{f,\lambda/8}^{Gauss,peak} = \frac{1-\nu}{1+\nu}\frac{C_p\,\rho\,\lambda}{8\,\alpha_L\sqrt{\tau}} = \frac{1-\nu}{1+\nu}\frac{C_p\,\rho\,\lambda}{8\,\alpha_L\sqrt{\tau}}, \tag{16}$$

which gives the same result as Eq. (8) when we replace q with q_0 in Eq. (8).

The critical heat flux factor for a temperature increase to 520°C is same as for the uniform laser exposure: $Q_{f,\Delta T=520°C} = \frac{\kappa}{2}\sqrt{\frac{\pi}{\alpha}}\Delta T_{max} = \frac{\sqrt{\pi\kappa c_p\,\rho}}{2}\Delta T_{max}$. (17)

Unlike uniform surface heating, which raises the temperature evenly, heating with a Gaussian profile can create shear stress in the near-surface region of the metal due to the nonuniform temperature distribution. The critical shear stress is determined from Eqs. (A4) and is

$$\sigma_{rz} = -\frac{E\alpha_L}{1-\nu}\frac{2}{k}\sqrt{\frac{\alpha}{\pi}}q_0\sqrt{\tau}\,\frac{\sqrt{\alpha\tau}}{R}\,\frac{n^{5/2}}{8}\sqrt{\frac{\pi}{e}} = \sigma_t\,\frac{\sqrt{\alpha\tau}}{R}\,\frac{n^{5/2}}{8}\sqrt{\frac{\pi}{e}} \approx 0.05\sigma_t \tag{18}$$

where σ_t is the transverse stress in both orthogonal directions parallel to the free surface (i.e., σ_{rr} and $\sigma_{\theta\theta}$), as described in Appendix A, Eq. (A6). Here is assumed $n=2$ and $\tau=3ms$.

The shear stress reaches its maximum within the heated layer and at the edges of the laser spot. In this analysis, we assume that the heated spot is small compared to the sample size, and that the surrounding cold material constrains lateral (radial) expansion, at least at the edges of the laser spot, so that the radial displacement is negligible (u≈0 and ∂u/∂z=0). From Eq. (18), it is evident that the shear stress is an order of magnitude smaller than the transverse stress. According to the Tresca and von Mises criteria, the critical shear stress is comparable in magnitude to the yield strength [13]. Therefore, the transverse stress remains the dominant factor controlling plastic deformation in the mirrors. We will thus focus on comparing the critical heat flux factors derived from the transverse stresses with the expected maximum heat flux for the mirrors. Please note that we applied the boundary condition ∂u/∂z=0, which is a very strict constraint. To verify our statement validity, we performed laser heat simulations of the mirror surface in ANSYS [14]. The results confirmed that the shear stresses are negligible compared to the transverse stresses.

Figures 2 and 3 show the critical heat flux factor for different materials $Q_{f,crit} = min\left\{Q_{f,[\sigma]}^{Gauss,peak}, Q_{f,\Delta T=520°C}\right\}$ that can be used as mirror substrate for the optical system. Heat fluxes below the maximum height of the green bars indicate conditions where the material shows no damage. The hatched (dashed) bars represent the $\lambda/8$ deformation limit, meaning the material deforms but remains within the acceptable tolerance (less than $\lambda/8$) up to the maximum height of the dashed

bars. Additionally, the vertical lines indicate the maximum heat flux factors for in-vessel mirrors (M1–M6) (Fig.2) and for ex-vessel mirrors (M7–M15) (Fig.3), all of which have a gold reflective coating. The maximum heat flux factors represent the peak heat flux values at the center of the laser spot with a Gaussian heat flux profile.

We can see that the maximum heat flux factors for ex-vessel mirrors (M7–M15) are significantly lower than those for the in-vessel mirrors. For these ex-vessel mirrors, the highest heat flux factor is reached at M12, with a value of *0.052 MW/m² $s^{1/2}$*. For most materials, $Q_{f,\lambda/8}^{Gauss,peak}$ is lower than the permanent damage threshold for a single-pulse operation mode. However, materials like recrystallized tungsten, annealed copper and aluminium experience plastic deformation before reaching *λ/8*. From Fig. 2, we can see that the commonly used material CuCrZr inside the ITER vacuum vessel is suitable as a substrate material. For the ex-vessel mirrors, which are subjected to lower heat fluxes, Zerodur can be used as a substrate, since its critical *λ/8* limit, $Q_{f,\lambda/8}$, is extremely high. Zerodur deforms only minimally and remains within the acceptable tolerance (less than *λ/8*) under all conditions.

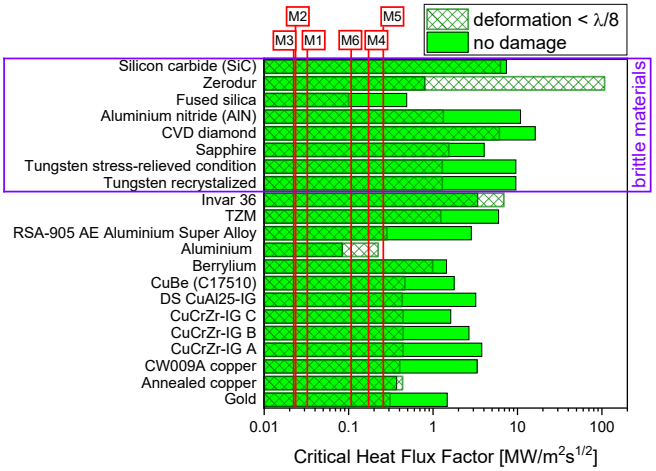

Fig. 2: Critical heat flux factors for various materials suitable as mirror substrates for high-power laser beam transport, based on a based on a Gaussian heat flux distribution. The red lines indicate the maximum heat flux factors for mirrors M1–M6 with gold coatings in the Port Plug.

Please note that the statements in Figures 2 and 3 are valid for both uniform and Gaussian heat flux distributions when we analysing the peak value at the laser spot center, where the transverse stresses are maximal. However, differences between the uniform and Gaussian profiles may become significant when considering the temperature distribution away from the center or when modeling thermal gradients.

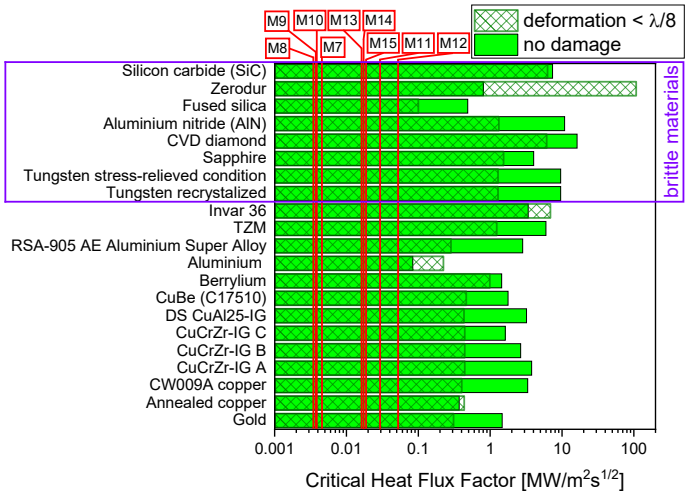

Fig. 3: Critical heat flux factors of potential mirror substrate materials under Gaussian laser irradiation. Red lines mark the maximum heat flux factors for ex-vessel mirrors (M7–M15) with gold coatings in the ISS and PCSS areas.

5.0 Thermal Load and Deformation Analysis of In-Vessel Mirrors Under Multi-Pulse Laser Operation

In operations with the maximum number of laser pulses, each pulse delivers a heat flux $\bar{q}$ to the target surface for a duration τ, and pulses are applied at a high repetition rate *f*. Rather than considering individual pulses separately, the cumulative thermal load over the measurement period can be described by the time average heat flux

$$\langle q\rangle = \bar{q}\cdot\tau\cdot f, \qquad (19)$$

which represents the effective steady-state thermal input to the surface. This approach captures the combined effect of all pulses, ensuring sufficient tritium release while keeping surface temperatures below critical deformation thresholds. In the T-monitor diagnostic design, operation is considered in different modes, with the most critical mode involving a high repetition of laser pulses, *f=64Hz*. In this mode, the laser delivers 192 pulses over a total measurement period of t_s*=3s* ($t_s=t_{scan}$). Each pulse has a duration of *1 ms* or *3 ms*, depending on the measurement conditions. The surface temperature raise for this mode can be given by:

$$\Delta T^{multi-pulse} = \frac{2}{\kappa}\sqrt{\frac{\alpha}{\pi}}\langle q\rangle\sqrt{t_s}\ F_{Gauss}(x_s,n) + \frac{2}{\kappa}\sqrt{\frac{\alpha}{\pi}}\bar{q}\sqrt{\tau}\ F_{Gauss}(0,n) =$$

$$= \frac{2}{\kappa}\sqrt{\frac{\alpha}{\pi}}\bar{q}\sqrt{\tau}\ F_{Gauss}(0,n)\left[1 + f\sqrt{\tau t_s}\right]\frac{F_{Gauss}(x_s,n)}{F_{Gauss}(0,n)} \qquad (20)$$

Where $x_s = \sqrt{\alpha t_s}/R = 1.17$ for t_s*=3s*. Therefore, the approximation $x \ll 1$ cannot be applied for multi-pulse operation. The second term in this equation represents the temperature rise during the last laser pulse. The critical temperature rise during the multi-pulse operation, at which transverse stresses reach the material's yield strength and plastic deformation begins, is represented by critical heat flux factor $Q_{f,[\sigma]}^{Gauss,mp}$. At the same time the $Q_{f,[\sigma]}^{Gauss}$ represents the critical heat flux factor required to achieve this critical temperature rise during a single laser pulse. Equation (20) can be rewritten

$$Q_{f,[\sigma]}^{Gauss,mp}\left[1+f\sqrt{\tau t_s}\right]\frac{F_{Gauss}(x_s,n)}{F_{Gauss}(0,n)}=Q^{Gauss}{}_{f,[\sigma]} \qquad Q_{f,[\sigma]}^{Gauss,mp}=Q_{f,[\sigma]}^{Gauss}\frac{1}{\left[1+f\sqrt{\tau t_s}\right]\frac{F_{Gauss}(x,n)}{F_{Gauss}(0,n)}} \qquad (21)$$

It follows that $Q_{f,[\sigma]}^{Gauss,mp}=\frac{Q_{f,[\sigma]}^{Gauss}}{3.35}$ and $Q_{f,[\sigma]}^{Gauss,mp}=\frac{Q_{f,[\sigma]}^{Gauss}}{2.36}$ for τ=3ms and τ=1ms respectively. Here is assumed $n=2$.

The critical heat flux for CuCrZr is 3 MW/m^2·s$^{1/2}$ as shown in Fig. 3. For multi-pulse operation, this flux is reduced by a factor of 3.35 to 0.9 MW/m^2·s$^{1/2}$. Nevertheless, it remains significantly above the maximum heat fluxes for the M1–M6 mirrors.

Multi-pulse operation leads to strong axial displacement of the mirror surface, as it is proportional to $\bar{q}t_s$. This results in the formation of surface bulges, which in turn cause beam defocusing. To avoid such defocusing, refocusing after each laser pulse is foreseen. Therefore, the axial displacement that must be considered is that produced by the last laser pulse, as defined by Eq. (7). Consequently, even in multi-pulse operation, the heat flux factors do not exceed the critical heat flux factor, $Q_{f,\lambda/8}^{Gauss,peak}$, corresponding to $\lambda/8$.

The in-vessel mirrors, designated M1 through M6, absorb varying levels of power per 3 ms laser pulse, ranging from 579 W for M1 to 710 W for M6, based on a surface reflectivity of 96%. Among these, the most critical parameter for thermo-mechanical performance is the maximal incident power density. The M4 mirror, which has the smallest laser spot

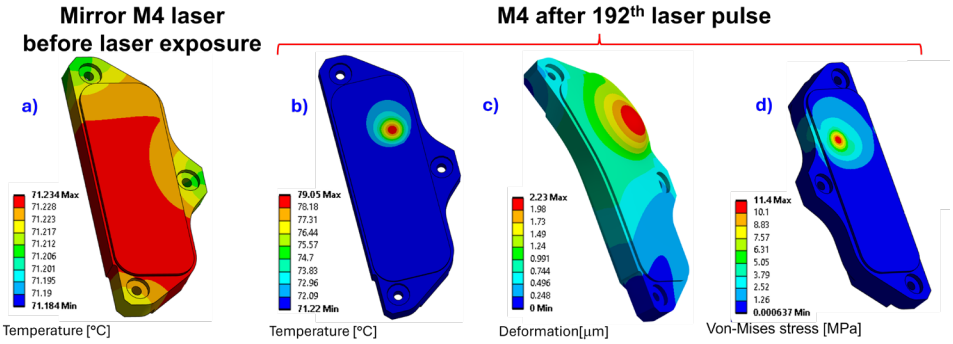

Fig. 4: (a) Temperature distribution after a 6-hour cooldown following plasma operation; (b) Temperature distribution after the 192nd pulse for M4; (c) Total deformation after the 192nd pulse (in micrometers, considering only laser load) d) Von-Mises stress.

footprint, is exposed to the highest loading of approximately 7.85 kW/cm². For M4, the absorbed power per pulse is 655 W, corresponding to a cumulative absorption of 377 J over 192 pulses.

Figure 4a shows the temperature distribution after a 6-hour cooldown following plasma operation, that is, before the operation of the T-monitor diagnostic. Figure 4b presents the temperature field at the end of the 192nd laser pulse. Prior to T-monitor measurements, the temperature of the M4 mirror is nearly uniform, with a deviation of less than 0.1 °C. After the 192-pulse sequence, the maximum temperature increase remains below 8 °C, which is comfortably under the plastic deformation threshold of annealed copper ($\Delta T_{threshold} \approx 11.3$ °C). Figure 4d further shows the resulting von Mises stress distribution, with a maximum value of about 11 MPa. Given that the yield strength of annealed copper is approximately 33.3 MPa, the expected stress after 192 laser pulses remains well below the material limit. This indicates that even under the most demanding conditions, the mirrors retain sufficient thermal and mechanical margin.

Figure 4c depicts the resulting total deformation of M4, considering only the laser load. Ray-tracing simulations performed in Zemax [15], using the deformed surface profile, demonstrate that optical performance is essentially unaffected compared to the nominal case. Minor spot displacements caused by surface distortion can be compensated through routine refocusing adjustments before subsequent laser pulses.

Overall, the analysis confirms that the in-vessel mirrors can withstand multi-pulse operation without permanent damage or unacceptable optical degradation. Since M4 represents the most critical loading scenario, the remaining mirrors (M1–M3, M5, M6) are expected to perform with even larger safety margins.

6.0 Summary and Material Selection for ITER T-Monitor Mirrors

This study assessed the thermo-mechanical performance of potential mirror substrate materials under the most critical laser loading scenarios, using both analytical modelling and numerical simulation. A simplified one-dimensional infinite half-space model was used to determine critical heat flux based on three operational limits: the permanent damage threshold (defined by yield stress for ductile materials and ultimate compressive stress for brittle ones), the gold coating temperature limit of 520 °C to prevent delamination, and the optical deformation limit of λ/8 at a wavelength of 1.07 μm to maintain image quality. Both uniform and Gaussian laser profiles were considered, and analytical predictions were validated with transient thermal and deformation simulations for representative in-vessel and ex-vessel mirrors. Thermal simulations for the highest-loaded mirror (M4) showed that, after 192 laser pulses of *3 ms* duration at 64 Hz, the maximum temperature rise remained below the plastic deformation threshold for annealed copper (≈8 °C vs. 11.3 °C limit). The stress in annealed copper after 192 laser pulses stays well below its 33.3 MPa yield strength. Predicted surface deformations did not significantly affect optical performance, with minor spot shifts correctable via refocusing.

Based on these results, materials with adequate safety margins were identified, providing a reliable framework for mirror durability under high-power, high-radiation conditions. The proposed optical design can maintain performance throughout T-monitor operation, supporting ITER's tritium inventory management and safety objectives.

7.0 Material Selection for the T-monitor Diagnostic system

Baseline Options:

- **CuCrZr + Au coating**: Selected for in-vessel mirrors and locations within the bioshield (cold dog leg) where high thermal loads are expected. The Au coating ensures high reflectivity and surface stability.
- **Zerodur + Au coating**: Chosen for areas exposed to lower beam power densities, providing dimensional stability and minimal thermal deformation. This material is also employed for the Fast Scanning Mirror Unit (FSMU) and Port Cell Support Structure (PCSS) optics.

Back-up Options:

- **CuCrZr or DS AL-25 with Cu intermediate plate + ZrO_2 protection layers**: Prevents Cu oxidation while maintaining structural and reflective properties.
- **Massive CuCrZr mirrors with polished surfaces**: Suitable for high thermal conductivity and mechanical robustness.
- **CuCrZr + ZrO_2 protection layers**: Provides enhanced oxidation resistance while preserving high thermal performance.

This material selection balances thermal performance, reflectivity, and structural stability, ensuring reliable mirror operation across varying environmental and laser-loading conditions

Acknowledgments

This work is supported by the ITER Organization under the Cooperation Agreement between Forschungszentrum Jülich GmbH and ITER (ref. IO/21/CT/4300002506). The views expressed do not necessarily reflect those of the ITER Organization.

Appendix A: Quasistatic Formulation of Thermoelastic Stresses in a Half-Space

In the quasistatic formulation, the problem of determining stresses in a half-space irradiated with an axisymmetric radiant flux can be described by the following strain–stress relations [8,9,10]:

$$\sigma_{rr} = \lambda\Delta + 2G\,(\partial u/\partial r) - \beta\Delta T \quad \text{(A1)}$$

$$\sigma_{\theta\theta} = \lambda\Delta + 2G\,(u/r) - \beta\Delta T \quad \text{(A2)}$$

$$\sigma_{zz} = \lambda\Delta + 2G\,(\partial v/\partial z) - \beta\Delta T \quad \text{(A3)}$$

$$\sigma_{rz} = G\,(\partial u/\partial z + \partial v/\partial r) \quad \text{(A4)}$$

where σ_{rr}, $\sigma_{\theta\theta}$, σ_{zz}, σ_{rz} are the radial, hoop, axial, and shear stresses, respectively; u, v are the radial and axial displacements; $\Delta = \varepsilon_{rr} + \varepsilon_{\theta\theta} + \varepsilon_{zz}$ is the dilatation; $\lambda = \nu E/[(1+\nu)(1-2\nu)]$ is Lamé's first parameter; $G = E/[2(1+\nu)]$ is the shear modulus; $\beta = (3\lambda + 2G)\alpha_L$; α_L is the coefficient of thermal expansion, ν is Poisson's ratio, E is Young's modulus; ΔT is the local temperature rise.The dilatation Δ consists of three normal strain components: radial strain $\varepsilon_{rr} = \partial u/\partial r$, hoop (circumferential) strain $\varepsilon_{\theta\theta}$=u/r around the axis, and axial strain $\varepsilon_{zz} = \partial v/\partial z$ along the surface-normal direction.

For the case of mirror irradiation with a pulsed laser, the following conditions apply:

- **Axisymmetric heating**: A laser beam typically produces a radially symmetric temperature profile on the surface.
- **Short timescale near the surface**: The laser rapidly heats the material, and surrounding cooler regions constrain radial expansion, limiting radial displacement near the irradiated spot.
- **Surface-normal deformation dominates**: Most of the expansion occurs along the z-direction **(**normal to the surface), so ε_{zz} is the dominant strain.
- **Essential boundary conditions at the axis ($r = 0$):**Axisymmetry imposes the following must conditions:
  - **Radial displacement zero at axis:** $u_r(0,z,t)=0$. (There is no jump or preferred radial direction at the axis.)
  - **Regularity of the gradient at $r = 0$.** The solution must be finite and smooth $\partial u_r/\partial r = 0$.
- **Top surface ($z = 0$, surface hit by laser):** The laser provides thermal loading, not mechanical traction (unless there is contact or pressure). For a free surface: **shear stress** $\sigma_{rz}(r,z=0,t)=0$; **normal stress** $\sigma_{zz}(r,z=0,t)=0$.

At the center of the spot on the surface, the governing equations reduce to:

$$\varepsilon_{zz} = \partial v/\partial z = \frac{(1+\nu)}{(1-\nu)}\,\alpha_L \Delta T \quad \text{(A5)}$$

$$\sigma_t = \sigma_{rr} = \sigma_{\theta\theta} = -\frac{E}{(1-\nu)}\,\alpha_L\,\Delta T \quad \text{(A6)}$$

where σ_t is the transverse stress in both orthogonal directions parallel to the free surface, (i.e., σ_{rr} and $\sigma_{\theta\theta}$). The transverse stresses are maximal at $r=0$. Finally, integrating Eq. (A5) over z yields the surface displacement:

$$v\,(r,0,t) - v\,(R,0,t) \approx -\frac{(1+\nu)}{(1-\nu)}\alpha_L \int_0^\infty \Delta T\,(r,z,t)\,dz \quad \text{(A7)}$$

The negative sign in the above expressions indicates compressive stress and surface displacement in the negative z-direction in response to heating.

Appendix B: Temperature Distribution for Gaussian Laser Heating of a Half-Space

The transient temperature field produced by a Gaussian laser heating of an elastic half-space ($z \geq 0$) is obtained from the Laplace-transformed heat equation [16]:

$$\Delta T^* - \frac{s}{\alpha} T^* = 0 \quad \text{(B1)}$$

where $T^*(r,z,s)$ is the Laplace transform of temperature,s is the Laplace variable (1/s), a is the thermal diffusivity (m^2/s), $\alpha = k/(\rho C_p)$. The surface boundary condition for a Gaussian flux is expressed as:

$$-k\frac{\partial T^*}{\partial z}\Big|_{z=0} = \frac{\bar{q}n^2}{2s}e^{-\frac{1}{2}\left(\frac{nr}{R}\right)^2} \quad \text{(B2)}$$

where $\bar{q}$ is the average laser heat flux and R is the nominal radius of the heated spot, n is Gaussian shape parameter (dimensionless). The quantity $q_0 = \frac{\bar{q}n^2}{2}$ represents the peak heat flux at the centre of the laser spot.

The Laplace-domain solution for the equation can be found in the form:

$$T^*(r,z,s) = \int_0^\infty A(s,\lambda)J_0(\lambda r)e^{-\gamma z}d\lambda\,, \quad \gamma = \sqrt{\lambda^2 + \frac{s}{a}} \quad \text{(B3)}$$

Here, λ is the radial transform (1/m), $\gamma = \sqrt{(\lambda^2 + s/a)}$ the Laplace-space decay rate, and $J_0$the order-0 Bessel function. The function $A(s,\lambda)$ is evaluated from the boundary condition using the Hankel transform for a gaussian source:

$$T^*(r,z,s) = \frac{\bar{q}R^2}{2k}\int_0^\infty \lambda e^{-\frac{1}{2}\left(\frac{R\lambda}{n}\right)^2} J_0(\lambda r)\frac{e^{-\gamma z}}{\gamma s}d\lambda \quad \text{(B4)}$$

Using the inverse Laplace transform the solution for the temperature distribution is obtained:

$$T(r,z,t) = \frac{\bar{q}R^2}{2k}\int_0^\infty e^{-\frac{1}{2}\left(\frac{R\lambda}{n}\right)^2} J_0(\lambda r)\left(\int_0^t g(t',\lambda,z)dt'\right)d\lambda \quad \text{(B5)}$$

where the function $g(t',\lambda,z)$ is given by the following expression: $g(t',\lambda,z) = \sqrt{\frac{\alpha}{\pi}}\sqrt{t'}\ \ exp\left[-\alpha\lambda^2 t' - \frac{z^2}{4\alpha t'}\right]$

Equation (B4) can be rewritten by swapping the order of integration using Fubini's theorem:

$$T(r,z,t) = \frac{\bar{q}R^2}{2k}\int_0^\infty \left[\sqrt{\frac{\alpha}{\pi}}\sqrt{t'}\ \exp\left(\frac{-z^2}{4\alpha t'}\right)\int_0^\infty e^{-\left(\frac{R^2}{2n^2}+\alpha t'\right)\lambda^2} J_0\,\lambda r)\,d\lambda\right]dt' = \frac{qR^2}{2k}\int_0^\infty \left[\sqrt{\frac{\alpha}{\pi}}\sqrt{t'}\ \exp\left(\frac{-z^2}{4\alpha t'}\right)I(t'r)\right]dt' \quad \text{(B6)}$$

$$\text{where}\quad I(t'r) = \int_0^\infty e^{-\left(\frac{R^2}{2n^2}+\alpha t'\right)\lambda^2} J_0\,\lambda r)\,d\lambda = \frac{1}{2\left(\frac{R^2}{2n^2}+\alpha t'\right)}exp\left(-\frac{r^2}{4\left(\frac{R^2}{2n^2}+\alpha t'\right)}\right) \quad \text{(B7)}$$

From this, we obtain the general formula for the temperature distribution in the eliminated material as a function of r, z, and τ where τ is the pulse duration of the laser:

$$T(r,z,\tau) = \frac{\bar{q}R^2}{4k}\sqrt{\frac{\alpha}{\pi}}\int_0^\tau \frac{dt\prime}{\sqrt{t'}\left(\frac{R^2}{2n^2}+\alpha t\prime\right)}exp\left[-\frac{z^2}{4\alpha t'} - \frac{r^2}{4\left(\frac{R^2}{2n^2}+\alpha t\prime\right)}\right] \quad \text{(B8)}$$

At the surface center (r=0, z=0), the solution reduces to a compact form:

$$T(0,0,\tau) = \frac{\bar{q}R^2}{4k}\sqrt{\frac{\alpha}{\pi}}\int_0^\tau \frac{dt\prime}{\sqrt{t'}\left(\frac{R^2}{2n^2}+\alpha t\prime\right)} \quad \text{(B9)}$$

Finally, it can be expressed as follows:

$$T(0,0,t) = \frac{2\bar{q}\sqrt{\alpha t}}{k\sqrt{\pi}}\left(\frac{n}{2\sqrt{2}x}tan^{-1}\left(\sqrt{2}nx\right)\right) = T_m(t)F_{Gauss}(x,n), \quad \text{(B10)}$$

where $x = \sqrt{\alpha t}/R$ is the normalized diffusion length, $T_m(t)$ is the characteristic maximum temperature scale for a uniformly heated half-space. $F_{Gauss}(x,n)$ is the dimensionless geometry factor describing Gaussian profile.

Here are the expressions for $T_m(t)$ and $F_{Gauss}(x,n)$: $T_m(t) = \frac{2\bar{q}\sqrt{\alpha t}}{k\sqrt{\pi}}$; $F_{Gauss}(x,n) = \frac{n}{2\sqrt{2}x}tan^{-1}\left(\sqrt{2}nx\right)$ (B11)

Studying the examining the extremes of the $F_{Gauss}(x,n)$ gives : $\lim_{x\to\infty} F_{Gauss}(x,n) = 0$; $\lim_{x\to 0+} F_{Gauss}(x,n) = \frac{n^2}{2}$

References

[1] Loarte A., Plasma Phys. Control. Fusion **67** (2025) 065023
[2] De Temmerman G. et al 2017 Nucl. Mater. Energy 12 267-272
[3] Klepper C. C. et al 2022 IEEE Trans. Plasma Sci. 50 /12 4970-4979.
[4] Friese S. et al., presented at the SOFT 2024 Conference
[5] Huber A. et al., Fusion Eng. Des. 219 (2025) 115298
[6] Huber A. et. al. submitted to the Nuclear Materials and Energy
[7] Blanchard J.P. Fusion Science and Technology 44 (2003) 101-105.
[8] Lee, K. H., Koumvakalis, N., & Bass, M. (1983). Thermoelastic stresses in solids irradiated by laser beams. Journal of Applied Physics, 54(10), 5727–5732. https://doi.org/10.1063/1.331794
[9] Parkus J., Thermoelasticity (Springer, New York, 1976).
[10] Hoyle R., in Thermal Stress, edited by B. P. Benham and R. Hoyle (Pitman, London, 1964).
[11] Carslaw H. S., Jaeger J. C., Conduction of heat in solids (2nd edition), Clarendon Press, 1959
[12] Ready J. F, Effects of High Power Laser Radiation (Academic, New York,1971).
[13] Cunha A., et al., J. Appl. Mech. Nov 2024, 91(11): 111008, https://doi.org/10.1115/1.4063894
[14] ANSYS, Inc., Canonsburg, PA, USA. [Online]. Available: https://www.ansys.com
[15] Ansys Zemax OpticStudio, https://www.ansys.com/products/ optics/ansys-zemax-opticstudio
[16] Parkus, Heinz. Instationäre wärmespannungen. Springer-Verlag, 1959